Pressure versus Heat-Induced Unfolding of Ribonuclease A: The Case of Hydrophobic Interactions within a Chain-Folding Initiation Site†

Joan Torrent,‡ James Patrick Connelly,§ Maria Gràcia Coll,‡ Marc Ribó,‡ Reinhard Lange,§ and Maria Vilanova*,‡

Laboratori d'Enginyeria de Proteïnes, Departament de Biologia, Facultat de Ciències, Universitat de Girona, Campus de Montilivi. E-17071 Girona, Spain, INSERM U128, IFR 24, 1919 Route de Mende (CNRS), F-34293 Montpellier, Cedex 5, France

Received June 25, 1999; Revised Manuscript Received September 21, 1999

ABSTRACT: To investigate the characteristics of the postulated carboxy terminal chain-folding initiation site in bovine pancreatic ribonuclease A (RNase A) (residues 106−118), important in the early stages of the folding pathway, we have engineered by site-directed mutagenesis a set of 14 predominantly conservative hydrophobic variants of the protein. The stability of each variant has been compared by pressure and temperature-induced unfolding, monitored by fourth derivative UV absorbance spectroscopy. Apparently simple two-state, reversible unfolding transitions are observed, suggesting that the disruption of tertiary structure of each protein at high pressure or temperature is strongly cooperative. Within the limits of the technique, we are unable to detect significant differences between the two processes of denaturation. Both steady-state kinetic parameters for the enzyme reaction and UV CD spectra of each RNase A variant indicate that truncation of hydrophobic side chains in this region has, in general, little or no effect on the native structure and function of the enzyme. Furthermore, the decreases in free energy of unfolding upon pressure and thermal denaturation of all the variants, particularly those modified at residues 106 and 108, suggest that the hydrophobic residues and side chain packing interactions of this region play an important role in maintaining the conformational stability of RNase A. We also demonstrate the potential of Tyr115 replacement by Trp as a non-destabilizing fluorescence probe of conformational changes local to the region.

Protein unfolding has gained a lot of interest in the past few years. This is partly driven by the biotechnological potential of enzymes withstanding extreme conditions and the pathological role of partly denatured proteins in a variety of diseases. However, despite numerous studies, no generally accepted mechanistic model is available. Protein unfolding has been variously described as a two-state or a multi-state process comprising several intermediates (*1*, *2*). Other authors have dismissed the idea of defined intermediates and explained experimental as well as simulation data in terms of more or less rugged conformational landscapes allowing multiple pathways from the folded to the unfolded form (*3*). These often contradicting views are easily explained by three factors: (a) due to the complexity of the macromolecular nature and the diversity of proteins, the experimental interpretation is necessarily model dependent; (b) different detection methods, such as NMR,[1] CD, fluorescence, etc., are likely to focus on particular unfolding events; (c) protein unfolding is induced by changes in different parameters, mainly by chemical denaturants, by heat or cold, and by pressure. While the use of chemical denaturants has the disadvantage that thermodynamic parameters have to be extrapolated from zero denaturant concentration, and it is often difficult to specify the precise interaction of the chemical agent with the protein, the use of heat is hampered by the fact that many proteins precipitate at high temperature or undergo irreversible structural changes. Pressure is a much less used effect that provides an elegant alternative, as it perturbs (within a limited range) chemical equilibrium reversibly. As most of the protein unfolding studies to date have been undertaken by the use of chemical denaturants or heat, it is of interest how the pressure data can be connected to them. This issue has been addressed most extensively in the case of staphylococcal nuclease wild-type and several variants by Royer and co-workers (*4*−*8*).

† This work was supported by Grants PB96-1172-CO2-02 from the DGES of the Ministerio de Educación y Cultura, Spain, and ACI-96-49 and ACI-97-20 from the CIRIT of the Generalitat de Catalunya, Spain. J.T. thanks the CIRIT of the Generalitat de Catalunya, Spain, for a short-term fellowship. J.P.C. was a Poste Vert (INSERM) postdoctoral fellow (1996-1998). Support was also received from the "Fundació M. F. de Roviralta" of Barcelona for equipment purchasing grants.

* To whom correspondence should be addressed. Fax: +34-972-418-150. E-mail: dbmvb@fc.udg.es.

‡ Universitat de Girona.

§ CNRS.

[1] Abbreviations: NMR, nuclear magnetic resonance; CD, circular dichroism; RNase A, bovine pancreatic ribonuclease A; CFIS, chain-folding initiation site; U_s^{II} and U_{vf} are unfolded species of RNase A corresponding to the major slow and the very fast refolding phases, respectively; C-terminal, carboxy-terminal; PCR, polymerase chain reaction; Tris, tris(hydroxymethyl)aminomethane; AcOH, acetic acid; FPLC, fast protein liquid chromatography; SDS−PAGE, sodium dodecyl sulfate−polyacrylamide gel electrophoresis; HPLC, high-performance liquid chromatography; MES, 4-morpholineethanesulfonic acid; CDA, cumulative difference amplitude; UV, ultraviolet; poly-(C), poly(cytidylic acid); C>p, cytidine 2′:3′-cyclic monophosphate; ATEE, *N*-acetyl-L-tyrosine ethyl ester; FTIR, Fourier transform infrared.

10.1021/bi991460b CCC: $18.00
Published on Web 11/09/1999

We thought it useful therefore to compare the thermodynamics of pressure and heat-induced unfolding for a series of closely related proteins. The model protein chosen had to meet two requirements: the unfolding reaction must be reversible for both pressure and temperature and—to simplify the analysis—the different proteins must be virtually identical but differing in only one parameter affecting their stability. A suitable model appeared to be a series of 14 variant forms of bovine pancreatic ribonuclease A (RNase A; EC 3.1.27.5) that differ in single-point amino acid substitutions within a hydrophobic chain-folding initiation site (CFIS). These sites correspond to elements of structure that are formed early in the folding pathway of proteins (*9*). RNase A has been extensively studied structurally and functionally (*10*, *11*). The equilibrium unfolding (*12*) and folding kinetics (*13*) of the wild-type and several variants has been characterized as a function of temperature and chemical denaturant, and in the case of the wild-type the addition of pressure-induced unfolding studies has allowed a phase diagram to be constructed (*14*−*16*). RNase A provides one of the best-studied examples of disulfide bond formation (of which it has four, involving all eight of its cysteine residues) and cis−trans isomerization (around the four X-Pro peptide bonds). As a consequence of the profound influence of cysteine and proline residues on protein-folding studies, rather less interest has focused on the role of CFIS in directing RNase A folding.

For RNase A, the existence of several CFIS that induce the formation of short hairpin-like conformations in the initial stages of the folding process has been postulated (*17*, *18*). There is evidence that one of the most probable CFIS extends from residue 106 to 118 (of 124) (*19*, *20*), a highly hydrophobic region of the protein that constitutes a β-hairpin in the native state, as illustrated in Figure 1. This region is highly conserved among the ribonuclease superfamily (*22*) with respect to the amino acid sequence and polarity, and this together with the high degree of protection from exchange, shown by its amide protons during unfolding, in hydrogen-exchange NMR experiments (*16*, *23*−*26*) may corroborate the importance of the region in initiating protein folding. It is now accepted that the initially formed hairpin structure is in rapid equilibrium with the unfolded state promoting the initial non-rate-limiting step, and recent double jump pulse labeling NMR experiments demonstrated its role during folding (*27*, *28*). Despite the diversity of multiple refolding phases arising from the rate-limiting cis−trans prolyl peptide isomerization, the folding pathways of the predominant slowly folding (U_s^{II}) and the very fastest folding (U_{vf}) species both show early folding intermediates with some structural order involving the 106−118 residue region. High-pressure NMR (*16*) also provides evidence of the enduring cohesion of the region as the protein unfolds.

In this paper, we compare the thermodynamics of pressure- and heat-induced unfolding of RNase A wild-type, from both natural and recombinant sources, and 14 variant forms of its 106−118 region. These single point variants were designed to change the residue hydrophobicity and size, with the exception of an amino acid replacement at position 115. To minimize structural rearrangement and the contribution of steric effects, most amino acid substitutions in this study are designed to be conservative, nondisruptive deletions so that the larger nonpolar side chains of residues in the C-terminal CFIS are systematically truncated. Since these types of amino acid substitutions shorten the hydrophobic side chain instead of modifying its shape, we assume that the results can be interpreted in terms of loss of side chain atoms, interactions, and local side chain relaxation or solvent intervention to accommodate the nominal cavity. Two Ile to Leu replacements were also investigated. These isomeric side chains have almost identical volume but different topologies: Leu is effectively different in the position of branching, and hence it would be expected to disrupt the local side chain environment and provide complementary information on the local flexibility. Furthermore, on the solvent-exposed exterior of the CFIS β-turn lies Pro114-Tyr115. At this position, more remote from the CFIS hydrophobic core, replacement of Tyr115 with Trp is expected not to perturb stability significantly. Trp115 may potentially serve as a unique and nondestabilizing fluorescent

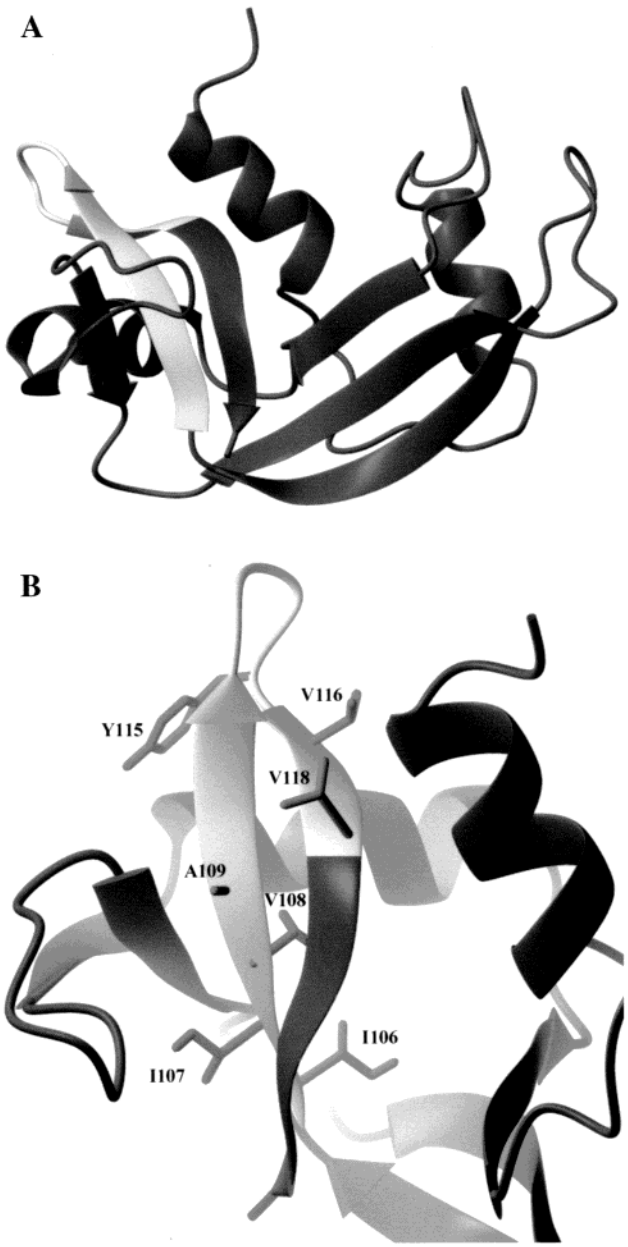

FIGURE 1: (A) Schematic representation of the three-dimensional structure of RNase A showing the location of the postulated CFIS (light gray). (B) View of the C-terminal β-hairpin showing the side chains of the hydrophobic residues substituted in this study. The figure was produced using the program MOLMOL (*21*).

label reporting on the CFIS as well as the conformational state and kinetics of the neighboring cis proline peptide bond.

For RNase A, our data provides information on the role of the CFIS in the stability of the protein and the starting point for kinetics investigations to probe the role of the region in protein folding. We also consider the potential of pressure as a tool for characterizing amino acid replacements. To the best of our knowledge, this is the first direct comparative characterization of the stability of an extensive set of variants using pressure- and temperature-induced protein unfolding under identical experimental conditions.

EXPERIMENTAL PROCEDURES

Purification of Wild-Type Ribonuclease A. Bovine pancreatic ribonuclease A (type I-A) purchased from Sigma Chemical Co. was further purified by cation-exchange chromatography as previously described (*29*).

Mutagenesis, Protein Expression, and Purification. The gene that encodes RNase A (*30*) was used as a template for the mutagenesis by PCR following a method previously described (*31*). Mutant and wild-type genes were expressed in *Escherichia coli* strain BL21(DE3) using the T7 expression system, and the encoded proteins were purified essentially as described by Raines and co-workers (*32*) with the following modifications: denatured and reduced protein, at a concentration of 0.3 mg/mL in 0.1 M Tris−AcOH buffer, pH 8.0, was oxidized using a mixture of reduced and oxidized glutathione (3.0 mM reduced, 0.6 mM oxidized). The resulting solution after concentration by ultrafiltration was dialyzed exhaustively against 20 mM Tris-HCl, pH 8.0, and then loaded onto an FPLC Mono S HR 5/5 cation-exchange column equilibrated with 20 mM Tris-HCl, pH 8.0. This step was found to be necessary to observe reversible unfolding transitions, probably by eliminating misfolded protein (i.e., scrambled isoforms lacking some disulfide bond) that easily could be generated during the refolding step of the purification protocol. Protein purity and homogeneity was confirmed by SDS−PAGE and by cation exchange as well as reversed-phase HPLC, using a Mono S HR 5/5 and a 214TP Vydac C4 column, respectively. Protein concentration was routinely determined spectrophotometrically using a molar extinction coefficient at 277.5 nm of 9800 M^{-1} cm^{-1} (*33*). The extinction coefficient of the Y115W variant was determined using a method previously described (*34*) and at 278 nm was found to be 14800 M^{-1} cm^{-1}. By this means, the following RNase A variants were prepared: I106A/L/V, I107A/L/V, V108A/G, A109G, Y115W, V116A/G, and V118A/G.

Absorption Spectroscopy. The proteins were dissolved to a concentration of 1 mg/mL in 50 mM MES buffer at pH 5.0 for pressure experiments and in 50 mM sodium acetate buffer, pH 5.0, for thermal experiments. These buffers were selected for their relatively small pressure and thermal pH dependencies, respectively. Absorption spectra between 250 and 310 nm were recorded in steps of 0.1 nm (1 nm bandpath) as a function of temperature at room pressure or under pressures up to 450 MPa at 40 °C, using the modified Cary3 (Varian) absorption spectrometer described elsewhere (*35*). All pressure experiments were done at 40 °C, which allowed most of the transition curve for each protein to be determined within the pressure limitation of our apparatus. Following each pressure or temperature increment, typically in steps of 20−50 MPa or 2−5 °C, respectively, the protein absorption was observed to equilibrate well within a 5-min pause before each measurement. Each spectrum was corrected for the pressure- or temperature-dependent change in volume before calculating the 4th derivative as previously described (*35*), optimized for Tyr or in the case of the Y115W variant for Trp. However, rather than determine the transition from amplitudes at a single wavelength, a method has been developed to exploit the whole spectral region and determine an averaged transition with a corresponding improvement in signal-to-noise ratio. First, a reference spectrum—usually the folded state 4th derivative spectrum at room conditions—was subtracted from each 4th derivative spectrum yielding a characteristic sinusoidal difference spectrum. Second, for each difference spectrum, the characteristic zero crossing point positions within the 275−290-nm range, typical of Tyr effects (or 290−295-nm range for Trp) were found, and the areas under the curve between each successive pair of zero points were calculated by summing the amplitude at each point. The absolute values of these sums were then added to give the cumulative difference amplitude (CDA). For spectra only slightly perturbed from the reference spectrum, the difference spectrum is very close to zero, and the noise may introduce many zero crossing points. To avoid summing up between spurious zero crossing positions in this case, the characteristic zero crossing points were imposed from the first difference spectrum where they could be determined consistently. Although the first step of taking the difference spectrum resulted in a decrease in signal-to-noise, this was minor as compared with the improvement associated with summing the amplitudes.

Fluorescence Spectroscopy. Fluorescence measurements of Y115W variant were made using an Aminco-Bowmann Series 2 luminescence spectrometer (SLM), modified to accommodate a pressure cell. Protein concentrations of 0.15 mg/mL in the same buffers as for absorption were used for pressure and temperature measurements, and solutions were placed in a 5 mm diameter quartz cuvette. Trp fluorescence was measured by exciting at 295 nm (8 nm slit) and emission being recorded between 310 and 400 nm (4 nm slit, 1 nm step size). Following baseline correction, spectra were analyzed by calculating the center of spectral mass (*36*) and the total fluorescence intensity registered between 315 and 400 nm.

Circular Dichroism Spectroscopy. To characterize the folded states of each protein, CD spectra were recorded at 10 °C using a Jasco-J715 spectropolarimeter equipped with a thermostated cell holder. All proteins were dissolved in 10 mM sodium cacodylate buffer, pH 5.0, and filtered using a 0.2-μm Millipore filter. A 0.01-cm optical path length quartz cell was used to record spectra of proteins in the far-ultraviolet region (180−260 nm) at a protein concentration of 1 mg/mL. For measurements in the near-UV region (250−310 nm), a 0.2-cm optical path length cell and a protein concentration of 0.5 mg/mL were used. All CD spectra were acquired at a scan speed of 20 nm/min, a 2 nm bandwidth, and a response time of 1 s. The sample compartment and the sample solution were purged with pure dry nitrogen. Spectra were signal-averaged over four scans. The solvent dichroic absorbance contribution was subtracted using the

Jasco software. The far-UV CD spectra were deconvoluted using the DICHROPROT suite of programs (*37*).

Determination of Steady-State Kinetic Parameters. Spectrophotometric assays (*38*) were used to determine the kinetic parameters for the cleavage of poly(C) (Sigma Chemical Co.) and the hydrolysis of cytidine 2′:3′-cyclic monophosphate (C>p) (Sigma Chemical Co.) by RNase A wild-type and variants. For C>p, the concentration of enzyme was 0.1 μM, the initial concentration of C>p was 0.1−3 mM, and the activity was measured by recording the increase in absorbance at 296 nm [$\epsilon_{296} = 516.4\ M^{-1}\ cm^{-1}$ (*38*)]. For assays of poly(C) cleavage, the concentration of enzyme was 5 nM, the initial concentration of poly(C) was 0.1−2.5 mg/mL, and the decrease in absorbance at 294 nm was monitored. All assays were carried out at 25 °C in 0.2 M sodium acetate buffer, pH 5.5, using 1-cm path length cells for C>p and 0.2-cm path length cells for poly(C). Steady-state kinetic parameters were obtained by nonlinear regression analysis using the program ENZFITTER (*39*).

Molecular Modeling. To gain structural insight into the effect of amino acid substitution and to correlate changes in interactions and stability, the different RNase A variants were modeled and superimposed on the wild-type structure. The variant models were generated with the TURBO-FRODO program (*40*) based in the RNase A protein crystal structure (PDB code: 7rsa) (*41*). Energy minimization of the wild-type structure and the variant models without water molecules was performed with the program GROMOS (*42*) for 10 runs of 1000 steps each. Optimized models were superimposed and solvent-accessible surfaces were calculated using the XAM program (*43*). Packing densities were estimated by counting the number of carbon atoms at a distance of less than 6 Å of the methyl carbon atom affected by substitution. Secondary structures were assigned with the DSSP program (*44*).

RESULTS

The 4th derivative method used here has been optimized for effects in the tyrosine spectrum. Although the more conventional second derivative method eliminates problems associated with baseline shifts and allows selective enhancement of the changes occurring in the 260−300-nm aromatic spectral region; the 4th derivative method allows greater selective enhancement. Optimized conditions can be found for resolving Tyr absorption changes in the presence of other absorbing species and possibly individual contributions among the six Tyr in RNase A. Phe is substantially blue shifted from the Tyr maximum and contributes little to the absorption as do the cystine bridges. Only in the case of the Y115W variant is there a substantial overlapping contribution from the tryptophan. Typical 4th derivative spectra following the increase of pressure or temperature on V116A are shown in Figure 2A,B. Pressure and temperature induce a blue shift and change in absorption that reflects the increase in polarity in the tyrosine environment due to solvation as the protein unfolds (*45*).

Fourth derivative spectral progressions with pressure or temperature for all RNase A variants show a major isosbestic point around 284 nm. With increasing temperature (Figure 2B), up to two further subsidiary isosbestic points involving only the first few (near native state) or last few (unfolded state) spectra can be observed. The corresponding CDA absorption change shows a sigmoidal transition, preceded and followed by (near linear) curves, as illustrated in the insets to Figure 2A,B. These slopes correspond to changes in the extinction coefficient and near-linear shifts of the intrinsic tyrosine spectrum in response to temperature, pressure, and solvent dielectric constant before or after protein unfolding. In the case of pressure up to 450 MPa, the intrinsic Tyr shift is negligible with our experimental resolution, and only a change in the fourth derivative amplitude is evident. With temperature, the shift disperses the major isosbestic point and introduces the two minor isosbestic points, reflecting thermally induced changes intrinsic to the Tyr spectrum in the native or unfolded states. This corresponds well with our recent observation of thermally induced isosbestic points in the 4th derivative spectra of ATEE (a model for tyrosine residues in proteins) in water or ethanol, accompanied by a decrease in absorption and a red shift with increasing temperature. As a result, the minor isosbestic points are not considered to represent any effect in the unfolding process. We conclude that the major

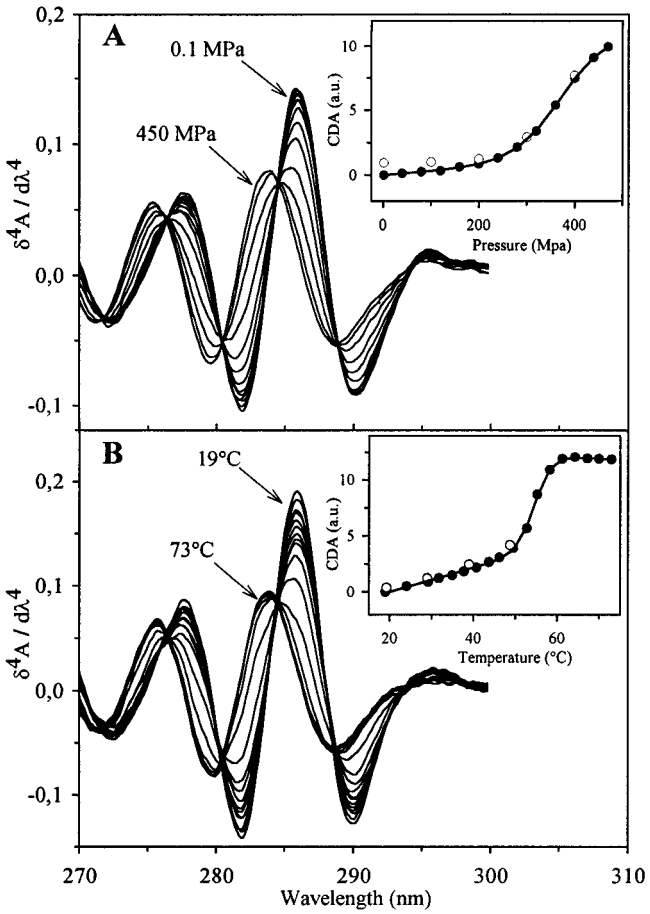

FIGURE 2: (A) Fourth derivative UV spectra of V116A as a function of pressure between room pressure and 450 MPa. Solution conditions: V116A at 1 mg/mL in MES buffer, 50 mM, pH 5.0, $T = 40$ °C. The inset shows the pressure unfolding curve for this RNase A variant. (B) Fourth derivative UV spectra of V116A as a function of temperature between 19 and 73 °C. Solution conditions: V116A at 1 mg/mL in sodium acetate buffer, 50 mM, pH 5.0, $P = 0.1$ MPa. The inset shows the temperature unfolding curve for this RNase A variant. The CDA was plotted upon increasing (filled circles) and decreasing (open circles) pressure (A) and temperature (B). Solid line is the nonlinear least-squares fit of the data based on a two-state model.

Table 1: Thermodynamic Parameters Calculated from Pressure Denaturation Curves of Wild-Type RNase A and Its Variant Forms at 40 °C and 0.1 MPa[a]

protein[b]	ΔG_U (kJ mol^{-1})	ΔV(cm^3 mol^{-1})	$P_{1/2}$(MPa)	λ_N(nm)[c]	λ_D(nm)[d]
WT	23.24 (0.44)	−46.5 (3.3)	500	285.8	285.6
recombwt	24.61 (0.70)	−46.5 (fixed)	529	285.4	285.0
Y115W abs	18.12 (1.39)	−43.2 (4.4)	419	285.6	284.1
Y115W fluor	19.66 (0.44)	−47.6 (1.2)	413		
I106A	2.50 (0.50)	−63.4 (3.8)	39	284.4	283.7
I106L	12.72 (0.58)	−47.7 (1.7)	267	285.4	283.6
I106V	17.42 (0.91)	−52.8 (2.7)	330	285.5	283.7
I107A	9.89 (0.35)	−47.4 (2.3)	209	285.5	283.7
I107L	11.60 (0.36)	−47.5 (1.0)	244	285.5	283.6
I107V	23.75 (2.3)	−52.2 (6.9)	455	285.9	285.1
V108A	3.13 (0.30)	−55.9 (2.7)	56	285.2	283.5
V108G[e]				283.8	283.8
A109G	23.72 (1.23)	−53.2 (3.4)	446	285.6	284.7
V116A	20.04 (0.52)	−53.6 (1.5)	374	285.8	284.0
V116G	18.41 (1.30)	−57.9 (3.8)	318	285.4	283.3
V118A	16.25 (1.31)	−51.2 (3.9)	317	285.3	283.6
V118G	11.90 (1.48)	−55.1 (4.8)	216	284.9	283.5

[a] Numbers in parentheses are the standard errors of the data. [b] WT, wild-type, corresponds to the natural (not recombinant) RNase A; Recomb WT, recombinant wild-type; abs, absorbance; fluor, fluorescence. [c] Wavelength of the 4th derivative amplitude maximum closest to the 283.5 nm isosbestic point and a pressure of 0.1 MPa. [d] Wavelength of the 4th derivative amplitude maximum closest to the 283.5 nm isosbestic point and a pressure of 440 MPa. [e] Completely denatured at 40 °C and 0.1 MPa.

Table 2: Thermodynamic Parameters Calculated from Thermal Denaturation Curves of Wild-Type RNase A and Its Variant Forms at Midpoint Transition and 0.1 MPa[a]

protein[b]	$\Delta H_{T_{1/2}}$ (kJ mol^{-1})	$T_{1/2}$ (°C)	$\Delta G_{U_{40°C}}$ (kJ mol^{-1})[c]	λ_N (nm)[d]	λ_D (nm)[e]
WT	487 (9)	58.9 (0.0)	24.76 (0.52)	286.1	284.3
recomb WT	437 (12)	58.0 (0.1)	21.16 (0.67)	285.5	283.9
Y115W abs	416 (19)	54.2 (0.1)	16.39 (0.82)	284.6	283.3
Y115W fluor	378 (17)	55.3 (0.2)	15.67 (0.81)		
I106A	301 (14)	43.1 (0.2)	2.87 (0.21)	285.7	283.7
I106L	410 (15)	51.7 (0.1)	13.68 (0.54)	285.7	283.7
I106V	431 (21)	55.0 (0.1)	17.81 (0.94)	285.7	283.8
I107A	405 (13)	47.7 (0.1)	9.26 (0.32)	285.3	283.8
I107L	435 (19)	49.4 (0.1)	11.98 (0.58)	285.3	283.6
I107V	422 (17)	58.6 (0.1)	20.83 (0.96)	285.7	283.7
V108A	350 (10)	43.3 (0.1)	3.59 (0.14)	285.6	283.7
V108G	237 (9)	29.4 (0.2)	−9.31 (0.37)	285.4	283.6
A109G	455 (21)	55.4 (0.1)	19.36 (0.98)	285.6	283.8
V116A	447 (27)	54.8 (0.2)	18.38 (1.22)	285.9	283.4
V116G	468 (52)	53.6 (0.1)	16.21 (0.57)	285.6	283.8
V118A	454 (89)	52.5 (0.1)	13.12 (0.60)	285.7	283.8
V118G	451 (58)	47.9 (0.1)	9.56 (0.36)	285.7	284.0

[a] Numbers in parentheses are the standard errors of the data. [b] See the explanations in Table 1. [c] Free energy of unfolding calculated at 40 °C. [d] Wavelength of the 4th derivative amplitude maximum closest to the 283.5 nm isosbestic point and a temperature of 25 °C. [e] Wavelength of the 4th derivative amplitude maximum closest to the 283.5 nm isosbestic point and a temperature of 75 °C.

isosbestic point observed for both increasing temperature and pressure indicates a two-state concerted unfolding process, and the spectrum is a weighted average of synchronous changes in the tyrosine spectral properties.

All unfolding transitions were observed to be reversible. Unfolding transition curves obtained from the CDA analysis were fitted to a two-state thermodynamic model combined with sloping linear functions for the native and denatured states as previously described (*45*). The fitted thermodynamic parameters for pressure-induced unfolding transitions are listed in Table 1 and for thermal transitions in Table 2. The free energy of unfolding for pressure has been measured relative to the folded state at 40 °C and 0.1 MPa. For comparison, ΔG_U for thermal unfolding, under the same conditions, has been calculated using eq 1 (*46*) and the fitted values of $\Delta H_{T_{1/2}}$ and $T_{1/2}$. The value for ΔC_p was fixed at 5.3 J K^{-1} mol^{-1} (*47*):

$$\Delta G_{U_T} = \Delta H_{T_{1/2}}(1 - T/T_{1/2}) - \Delta C_p[(T_{1/2} - T) + T \ln (T/T_{1/2})] \quad (1)$$

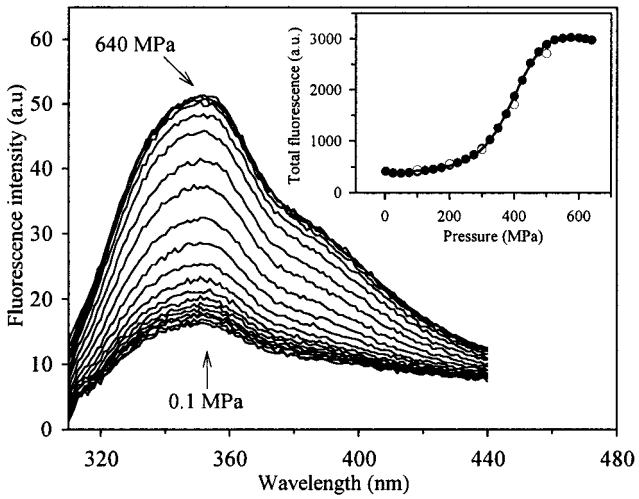

FIGURE 3: Fluorescence emission spectra of Y115W upon excitation at 295 nm (exciting only Trp) as a function of pressure between room pressure and 640 MPa. Solution conditions: Y115W at 0.15 mg/mL in MES buffer, 50 mM, pH 5.0, $T = 40$ °C. The inset shows the pressure unfolding curve for Y115W variant. The total fluorescence between 310 and 440 nm was plotted upon increasing (filled circles) and decreasing (open circles) pressure. Solid line is the nonlinear least-squares fit of the data based on a two-state model.

In the case of the Y115W variant, fluorescence as well as 4th derivative absorption was measured. Spectra showing the change in fluorescence with pressure are shown in Figure 3. A large increase in fluorescence yield and a red shift of the maximum around 350 nm is apparent. Plotting the total fluorescence emission (315−400 nm) against pressure or temperature yielded a transition curve that was fitted using the same two-state model as for the absorption results (Tables

1 and 2). As discussed elsewhere (*48*), the fit of the unfolding transition is limited by the precision to which the preceding and succeeding baseline curves can be determined. This was particularly notable for Y115W, and we attribute a significant part of the variation in ΔG_U between Tables 1 and 2 to this effect. Fluorescence center of spectral mass and 4th derivative absorption optimized for Trp gave a smooth curve with no apparent transition.

Relative changes among the variant ΔG_U values together with the $T_{1/2}$ or $P_{1/2}$ listed in Tables 1 and 2 give a consistent idea of the relative stabilities both among the different sites and also among different variants at the same site. Wild-type proteins, from both natural and recombinant sources, are virtually identical in behavior, so the process of refolding and purification from inclusion bodies does not significantly affect the stability. I107V and A109G are only slightly destabilized. The I106 variant proteins are less stable than their I107 analogues. Of the Val variants, the V108 series is most unstable while the V116 and V118 series are far less affected, V116 slightly less so than V118. Among the variants at each site, the stability follows in the order Ile > Val > Leu > Ala > Gly although the relative stabilities within each series varies a little, and I106L appears to be comparatively more stable than I107L within their respective series. For the Y115W variant, fluorescence gives similar thermodynamical parameters to 4th derivative absorption for pressure and thermal unfolding transitions. Its stability was found to be a little less than that of wild-type RNase A. Since the Trp115 fluorescence intensity change is sensitive to the local environment while the 4th derivative spectra reflect averaged more remote changes, this reinforces the conclusion that the unfolding process is concerted and apparently two state.

The steady-state kinetic parameters for the cleavage of poly(C) and the hydrolysis of C>p by the whole set of modified ribonucleases are very similar to the values found for the wild-type enzyme (results not shown). In most cases the differences are negligible (I106A/V, I107A/L/V, V108A/G and V116A), and for the others, the effect of amino acid replacement is small. As compared with the wild-type RNase A, only the I106L variant exhibited a small increase in the K_m value, while amino acid replacements A109G and V118A caused small changes in the K_{cat} value for the hydrolysis of C>p. For the cleavage of poly(C), we observed a small increase in the K_m parameter for RNase A I106L, V116G, V118A, and V118G and a small decrease in the value of $(V_{max}/[E_o])_{rel}$ for A109G variant as compared with the wild-type RNase A.

To discern if there are significant structural differences among the RNase A variants, CD spectroscopy has been used. Only small effects are observed in the CD spectra of the peptide and aromatic region on amino acid replacement, and these changes prove too small to discern any significant secondary structural changes by deconvolution. Values for the α-helix content, given in Table 3, are the best determined and agree well with the X-ray structure of RNase A (*41*). All spectra are virtually the same with the exception of V108G, illustrated in Figure 4. Qualitative analysis of the V108G CD spectrum suggests a general perturbation of secondary structure with respect to the wild-type. The blue shift of the maximum below 200 nm suggests increased random coil character at the expense of β-sheet.

Table 3: Changes in Various Parameters of Engineered C-Terminal Variants of RNase A

RNase A variant	α-helical content (%)	solvent-accessible area of wild-type side chain (Å^2)[a]	loss of solvent-ccessible area buried in folded protein (Å^2)[b]	no. of methyl(ene) groups + C_α atoms < 6 Å[c]
I106A	21.9	2.1	61.3	76
I106V	20.4	2.1	14.1	27
I106L	21.3	2.1	22.7	
I107A	20.7	19.7	50.6	58
I107V	19.5	19.7	4	18
I107L	21.8	19.7	12.3	
V108A	20.2	2.4	43.2	54
V108G	18.8	2.4	67.7	80
A109G	21.3	2.6	17.9	23
V116A	18.3	39.7	29	24
V116G	20.0	39.7	42.2	39
V118A	20.5	39.2	22.9	30
V118G	19.5	39.2	48.5	51

[a] The exposed area of the different target side chains in wild-type protein was calculated using the program XAM. [b] The difference in solvent-accessible area buried on folding between wild-type and each variant was calculated as previously described (*49*). [c] The number of methyl and methylene groups at a distance of less than 6 Å (packing density) was determined for each of the methylene groups deleted by amino acid substitution and then summed.

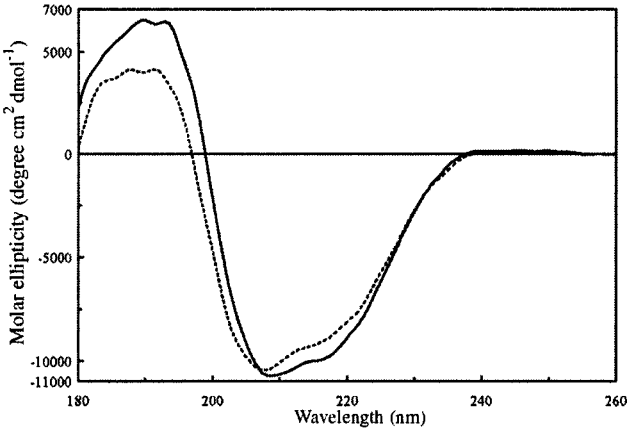

FIGURE 4: Circular dichroism spectra in the aromatic region of wild-type RNase A (solid line) and V108G variant (dotted line) at 36.5 μM in 10 mM sodium cacodylate, pH 5.0, at 10 °C.

Another indirect means to compare the variant and wild-type structures is to compare the wavelength of the maximum 4th derivative amplitude closest to the 284 nm isosbestic point. Measurements of these wavelengths for comparable conditions are listed in Tables 1 and 2. The native and unfolded state conditions for the pressure experiment at 40 °C are defined as 0.1 and 440 MPa, respectively, and for the thermal unfolding experiment (at room pressure) as 25 and 75 °C, respectively. The wavelength values reflect the polarity of the average environment about the Tyr residues, and on unfolding, there is a shift to the blue. There are roughly linear correlations between ΔG_U and the folded and unfolded state maximum amplitude wavelengths, but only in the case of the folded-state shift for the pressure data is the correlation significantly more than flat. This suggests that there are no exceptional cases, judging from the Tyr shift, in the variants and that only at 40 °C and 0.1 MPa is there a significant ratio of folded to unfolded protein present to produce an observable shift. From CD and absorption data

there is little evidence to suggest that any of the variants other than V108G, which however retains wild-type-like activity, have altered secondary structure as compared with wild-type protein.

We conclude that the only significant structural differences among the variant proteins are local to the CFIS; therefore, the variant CFIS structures can be modeled based on the wild-type structure. From these, local structural parameters can be estimated that relate to polarity and the role of hydrophobicity and van der Waals interactions at each residue site. These are listed in Table 3. The solvent-accessible side chain area and change in this parameter on folding give an indication of the importance of hydrophobicity at each site. The packing density gives an indication of the local polarity and role of van der Waals interactions (*50*).

DISCUSSION

Local or Global Structural Changes. In this study, we employ the Tyr residues to monitor the protein structure. Their spectral shifts and absorbance are a function of the environment. The folded and unfolded states are distinguished by the polarity of the Tyr side chain environments, which in the unfolded state are solvated to some degree while in the folded state reflect the environment in protein. According to a recent study on Tyr to Phe variants (*51*), the changes observed in absorption on unfolding are largely due to Tyr remote from the CFIS (38% to Tyr25, 13% to Tyr92, and 39% to Tyr97, leaving 10% to a fourth Tyr residue). As a result, the 4th derivative method does not provide local information on the CFIS region but rather a spectrum averaged over the predominantly remote Tyr and the mixture of conformations with different Pro isomers comprising the unfolded state.

Local information about the CFIS is rather provided by fluorescence changes. Tyr115 is largely solvent exposed at the bend of the CFIS hairpin. Replacement of the Tyr115 by Trp gives a unique fluorescence probe that shows a clear fluorescence intensity transition on unfolding, indicating changes in fluorescence efficiency, possibly due to local changes in static quenching conditions or hydrogen bonding. The characteristics of this transition show no significant difference from those of the absorption transition for both pressure and temperature unfolding, confirming that local and averaged transitions show a concerted behavior. There is no apparent transition indicated by the spectral shift (judged from the center of spectral mass) but rather a smooth curve. Analogous behavior is obtained for the 4th derivative absorption above 290 nm optimized for Trp, and this indicates that there is no significant change in polarity around Trp115 during unfolding. Since the Y115W amino acid replacement does not substantially perturb the stability (Tables 1 and 2), this suggests that this variant can serve as a reporter group for the Pro114 isomerization kinetics and for local effects in the CFIS.

Pressure versus Thermal Unfolding. It is notable that for all variants, we see a two-state reversible unfolding process for both pressure and temperature. An NMR study by Zhang et al. (*16*) of equilibrium pressure and temperature unfolding demonstrated, by following the four histidine residues, that different regions of the protein appear to unfold sequentially. Furthermore, they show that pressure and heat lead to different structures in the wild-type unfolded state (*16*). Pressure-induced protein unfolding appears to lead to a molten globule state (*16, 52*) where nativelike secondary structure is retained but solvent is admitted to the core regions of the protein. In contrast, the thermally unfolded state appears to be more extensively unfolded, as it shows a stronger increase in hydrogen exchange at internal residue sites (*16*). Further evidence of structural differences in the pressure- and heat-induced unfolded states comes from our recent FTIR study of the variant proteins (unpublished results).

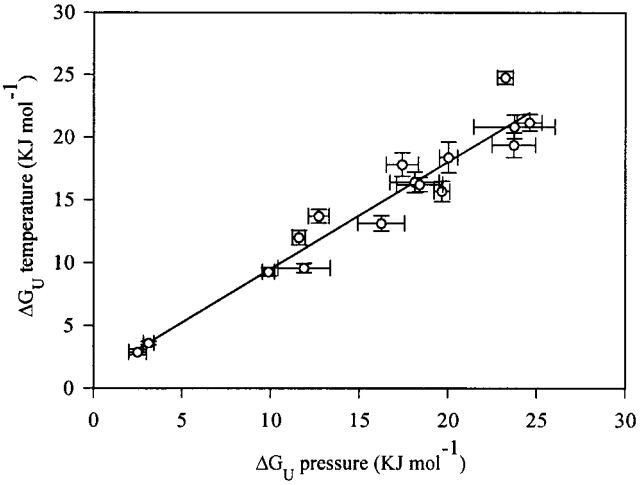

FIGURE 5: Correlation between the free energies of unfolding of each RNase A variant calculated from pressure and temperature denaturation curves at 40 °C and 0.1 MPa. The solid line show the best fit to a linear equation ($r = 0.965$). Error bars are standard errors of the data.

In light of this, it is interesting that we obtain virtually identical free energy of unfolding values from pressure and temperature unfolding experiments. Within our experimental errors, the ΔG_U values for all the variants are the same for pressure and temperature unfolding with respect to the same starting folded-state conditions, at 40 °C and 0.1 MPa (Figure 5). Other indicators of stability, the midpoint temperatures or pressures ($T_{1/2}$ and $P_{1/2}$) of unfolding correlate closely with ΔG_U and each other, showing that the thermodynamic parameters vary in an analogous way. This suggests a comparable and concerted unfolding mechanism for the whole series of protein variants and implies that the unfolding process monitored by the Tyr requires equivalent energy for pressure and temperature. Tyr fluorescence follows solvent ingress into the unfolding protein, and the Tyr are apparently in the same unfolded-state environment despite possible differences in the mechanism of unfolding. We may see a simple two-state unfolding process because the process is sufficiently concerted not to discern differences between Tyr environments that are averaged over different unfolded states, a possible result of using higher pH conditions. The equivalency in energy for this process under pressure, thermal, and chemical denaturation is not without precedent, as demonstrated by Royer and co-workers for staphylococcal nuclease (*4-8*). A note of caution should be made however. Prehoda et al. (*53*) have shown recently that neglect of the compressibility can result in artificially elevated values for ΔG_U and ΔV and this may systematically increase our pressure values, so the similarity with the thermal values may be coincidental. The slopes preceding and succeeding

Table 4: Average Values of Stability Losses for Equivalent Amino Acid Substitutions Made at Different Sites of the C-Terminal CFIS and Relationship with Changes in Solvent Transfer Values and Residue Volume Corresponding to These Amino Acid Replacements

		pressure denaturation		temperature denaturation			
type of substitution	no. of variants	$\Delta\Delta G_{U_{bur}}$ (KJ mol^{-1})[b]	$\Delta\Delta G_{U_{bur}}/CH_2$ (KJ mol^{-1})[c]	$\Delta\Delta G_{U_{bur}}$ (KJ mol^{-1})[b]	$\Delta\Delta G_{U_{bur}}/CH_2$ (KJ mol^{-1})[c]	ΔG_{tr} (KJ mol^{-1})[d]	$-\Delta V_{res}$ (Å^3)[e]
Ile-Ala	2	18.98	6.33	15.56	5.19	16.07	74.8
Ile-Val	2	4.12	4.12	1.88	1.88	5.69	25.8
Ile-Leu	2	13.28		8.90		−0.08	0.3
Val-Ala	3	12.34	6.17	10.17	5.09	10.38	49.0
Val-Gly	2[a]/3	11.14	3.71	17.26	5.75	14.60	75.3
Ala-Gly	1	0.89	0.89	1.81	1.81	4.27	26.3

[a] For pressure denaturation experiments. [b] Average $\Delta\Delta G_U$ value expected for each equivalent amino acid substitution made if the side chain was 100% buried. This value was calculated as previously described (*55*). [c] The average $\Delta\Delta G_{Ubur}$ values for the aliphatic side chains have been divided by the number of CH, CH_2, or CH_3 groups. [d] The ΔG_{tr} values corresponding to these amino acid substitutions are based on measurements for water → *n*-octanol (*56*) and have been corrected for the difference in volume between the solutes and solvents (*57*). [e] The $-\Delta V_{res}$ values are based on the volumes occupied by buried residues (*54*).

the pressure unfolding curves prevented a well-determined fit, including a change in compressibility. Regardless of the absolute values, the correlation between changes in stability to pressure and temperature observed for the variants shows that amino acid substitution is having analogous effect on pressure and thermal unfolding. Pressure appears to provide a useful alternative way to temperature to characterize protein stability.

Volume Changes. The observed ΔV changes (Table 1) on pressure unfolding for all variants are, in general, more negative than the wild-type protein and show roughly the same trend as the change in residue volumes in the interior of proteins $-\Delta V_{res}$, taken from Harpaz et al. (*54*), listed in Table 4. As discussed by Brandts et al. (*14*) and more recently by Royer and co-workers (*6*, *7*), the ΔV values observed are much smaller than the ΔV expected simply by analogy with volume changes on phase-transfer studies of amino acids and therefore reflect compensating changes. Frye and Royer (*7*) show that for staphylococcal nuclease wild-type and several variants, the effects due to electrostriction, compressibility, and hydration of exposed surface area on unfolding do not contribute significantly to the observed ΔV on pressure unfolding. The predominant effect appears to be attributable to the elimination of packing defects. For RNase A, we are unable to eliminate or estimate the contribution of compressibility or electrostriction to ΔV. Indeed, our choice of conservative cavity-forming hydrophobic variants results in relatively small changes in ΔV among the variants (all lie in the range 47−63 mL) and can be explained both by changes in the exposed surface area and by packing defects. However, as discussed below, the situation is quite different when we analyze the changes in free energy.

Hydrophobic Interactions. One aim of this study is to investigate the importance of hydrophobic interactions in the stability of the 106−118 residue region using cavity variants. Although the stability of the variants varies significantly, their activities are very similar, and this together with the CD results suggest that the folded state structures are very similar, with the possible exception of the V108G variant. This gives us confidence to compare the variants directly and interpret thermodynamic changes in terms of perturbations of the well-documented wild-type structure.

One means to judge the contribution of the hydrophobic effect to globular protein stability is by comparing the changes in variant stability relative to the wild-type protein ($\Delta\Delta G_U$) with the free energy change on transferring model amino acid side chain compounds from water to *n*-octanol (ΔG_{tr}). We have used the analysis of Pace (*55*) and corrected for variable solvent accessibility (given in Table 2) by scaling the experimental $\Delta\Delta G_U$ to the value for 0% solvent accessibility ($\Delta\Delta G_{U_{bur}}$). We find that the corrected transfer free energies (ΔG_{tr} listed in Table 4) agree quite well with the $\Delta\Delta G_{U_{bur}}$ values (listed in Table 4), expected for each equivalent amino acid substitution made, obtained from the pressure [$r = 0.929$ (5 data points)] and temperature measurements [$r = 0.978$ (5 data points)]. These results compare well with the combined analysis of barnase, staphylococcal nuclease, T4 lysozyme, and gene V protein variants probed by chemical denaturation ($r = 0.96$) (*55*). The changes induced by the variants indeed appear characteristically hydrophobic and conservative, with little evidence of unexpected structural or solvent compensating effects. The correlation between destabilization and ΔG_{tr} values does not extend to variants bearing nontruncation amino acid substitutions as Ile-Leu.

Expressed as the energetic cost of deleting one (Ile-Val), two (Val-Ala), or three (Ile-Ala) methyl(ene) groups from the CFIS, average values of $\Delta\Delta G_{U_{bur}}$ obtained from pressure and temperature denaturation divided by number of methyl(ene) groups, listed in Table 4, also compare well with values for equivalent amino acid replacements in other proteins (*49*, *55*, *58*). The mean reduction in the free energy of unfolding per deleted methyl(ene) group ($\Delta\Delta G_{U_{bur}}/CH_2$), upon pressure and temperature denaturation (excluding Gly variants), is found to be 5.54 and 4.05 kJ mol^{-1}. Nemethy et al. (*59*) noted that conformational entropy associated with Gly may reduce the $\Delta\Delta G_U$ changes involved. In this study, we observe a similar effect on $\Delta\Delta G_U$ for this type of hydrophobic substitution as compared to other replacements.

The change in free energy of unfolding is proportional to the solvent-accessible surface area of the side chains involved (*60*). We can therefore estimate the energy of burial of hydrophobic surface by dividing the change in stability for each variant relative to wild-type ($\Delta\Delta G_U$) by the change in the solvent-accessible surface area in solution, calculated from our models using the XAM program, for the hydrophobic side chains involved in amino acid substitution. This is a measure of the hydrophobic strength. Ile to Leu replacements were not taken into account. An average value

of 236 J mol^{-1} Å^{-2} for RNase A variants from pressure data and 218 J mol^{-1} Å^{-2} from temperature data compare well with 196 J mol^{-1} Å^{-2} from solute transfer measurements of model compounds (*57*), 229 J mol^{-1} Å^{-2} for CI2 protein (*58*), and 263 J mol^{-1} Å^{-2}, an average value found for barnase, staphylococcal nuclease, and gene V protein (*49*).

Steric Effects. It is apparent from Tables 1 and 2 that equivalent amino acid substitutions at different positions in the protein give rise to different values of $\Delta\Delta G_U$. These variations must be the result of variations in the environment surrounding the different residues, either from the solvent or the protein, as they do not result from differences in the hydrophobicity of the side chain. Experimental $\Delta\Delta G_U$ values obtained upon pressure and thermal denaturation are found to scale linearly with the difference in the side chain solvent-accessible area buried on folding between wild-type and variant proteins (Table 3), which is consistent with results reported for barnase (*49*) and CI2 protein (*58*). A significantly better correlation is found between $\Delta\Delta G_U$ and the packing density represented by the number of methyl(ene) groups plus the C_α atoms within a sphere of 6 Å radius of the hydrophobic group deleted (Table 3). This indicates that the packing density around a particular residue is important in determining the contribution the residue makes to protein stability.

Some of the differences in response to amino acid replacement at different sites may be explained structurally in terms of the importance of the side chain interactions between secondary structural elements. The two most important residues to stability, Val108 and Ile106, are both buried, and their side chains project into a central hydrophobic core. Val108 appears more strategically situated at the center of the hydrophobic region. These residues appear to promote secondary structural contacts and are among the more conserved in the region, suggesting that in this region, residue conservation may maintain a pattern of folding as much as specific structural interactions in the folded state. In contrast, Ile107 and Ala109 side chains project toward the solvent surface and, consequently, are more solvent exposed. The I106L variant is relatively more stable than its analogue I107L. Considering that the Ile106 side chain is more buried, the change in side chain shape might be expected to be more disruptive. This suggests that the Ile106 site is more able than Ile107 to accommodate structural changes. V118 residue site has a higher packing density than V116 site. Amino acid replacements at the former position result in more destabilized variants. Both sites are considerably more solvent accessible than residues 106−109.

Conclusion. UV absorbance and fluorescence spectra indicate that RNase A unfolds reversibly in a concerted mechanism without thermodynamic intermediates. Although heat and pressure are known to induce different structural changes, the changes in free energy, ΔG_U, are found to be identical within our detection limits. This holds for a series of 15 variant forms in a range from −9 to +25 kJ mol^{-1}. A comparison with model systems suggests that the differences in ΔG_U among the variants are attributable to both hydrophobic interactions (expressed as the energy of burial of hydrophobic surface) and the packing density. By a direct comparison of pressure- and heat-induced unfolding thermodynamics, the energetic changes produced by amino acid replacement in the 106−118 CFIS region could be better understood. Two particular residues (I106 and especially V108) are, among those analyzed, the most important sites for the RNase A stability. To obtain further and deeper insight into the mechanism of unfolding, the Y115W labeled variant can be expected to provide a useful probe for the folding/unfolding kinetics.

ACKNOWLEDGMENT

This work was undertaken in the frame of the European D10 action. The authors thank Ronald T. Raines for his generous gift of the gene that encodes RNase A and Claude Balny for helpful discussions and advice in the high-pressure experiments. We are also indebted to the "Servei de Biocomputació", I.B.F., Universitat Autònoma de Barcelona, Barcelona, Spain, for their help in molecular modeling.

REFERENCES

1. Ptitsyn, O. B. (1994) *Protein Eng. 7*, 593.
2. Walkenhorst, W. F., Green, S. M., and Roder, H. (1997) *Biochemistry 36*, 5795.
3. Chan, H. S., and Dill, K. A. (1998) *Proteins 30*, 2.
4. Royer, C. A., Hinck, A. P., Loh, S. N., Prehoda, K. E., Peng, X., Jonas, J., and Markley, J. L. (1993) *Biochemistry 32*, 5222.
5. Vidugiris, G. J. A., Truckses, D. M., Markley, J. L., and Royer, C. A. (1996) *Biochemistry 35*, 3857.
6. Frye, K. J., Perman, C. S., and Royer, C. A. (1996) *Biochemistry 35*, 10234.
7. Frye, K. J., and Royer, C. A. (1998) *Protein Sci. 7*, 2217.
8. Panick, G., Vidugiris, G. J. A., Malessa, R., Rapp, G., Winter, R., and Royer, C. A. (1999) *Biochemistry 38*, 4157.
9. Serrano, L., Matouschek, A., and Fersht, A. R. (1992) *J. Mol. Biol. 224*, 847.
10. D'Alessio, G., and Riordan, J. F., Eds. (1997) *Ribonucleases; Structures and Functions*, Academic Press, New York.
11. Raines, R. T. (1998) *Chem. Rev. 98*, 1045.
12. Pace, C. N., Laurents, D. V., and Thomson, J. A. (1990) *Biochemistry 29*, 2564.
13. Neira, J. L., and Rico, M. (1997) *Folding Des. 2*, R1.
14. Brandts, J. F., Oliveira, R. J., and Westort, C. (1970) *Biochemistry 9*, 1038.
15. Zipp, A., and Kauzmann, W. (1973)*Biochemistry 12*, 4217.
16. Zhang, J., Peng, X., Jonas, A., and Jonas, J. (1995) *Biochemistry 34*, 8631.
17. Matheson, R. R., and Scheraga, H. A. (1978) *Macromolecules 11*, 819.
18. Nemethy, G., and Scheraga, H. A. (1979) *Proc. Natl. Acad. Sci. U.S.A. 76*, 6050.
19. Beals, J. M., Haas, E., Krausz, S., and Scheraga, H. A. (1991) *Biochemistry 30*, 7680.
20. Dodge, R. W., and Scheraga, H. A. (1996) *Biochemistry 35*, 1548.
21. Koradi, R., Billeter, M., and Wüthrich, K. (1996) *J. Mol. Graphics 14*, 51.
22. Beintema, J. J., Breukelman, H. J., Carsana, A., and Furia, A. (1997) in *Ribonucleases; Structures and Functions* (D'Alessio, G., and Riordan, J. F., Eds.) pp 245−269, Academic Press, New York.
23. Talluri, S., and Scheraga, H. A. (1990) *Biochem. Biophys. Res. Commun. 172*, 800.
24. Robertson, A. D., and Baldwin, R. L. (1991) *Biochemistry 30*, 9907.
25. Nash, D., Lee, B. S., and Jonas, J. (1996) *Biochim. Biophys. Acta 1297*, 40.
26. Neira, J. L., Sevilla, P., Menéndez, M., Bruix, M., and Rico, M. (1999) *J. Mol. Biol. 285*, 627.
27. Udgaonkar, J. B., and Baldwin, R. L. (1995) *Biochemistry 34*, 4088.
28. Houry, W. A., and Scheraga, H. A. (1996) *Biochemistry 35*, 11734.

29. Alonso, J., Nogués, M. V., and Cuchillo, C. M. (1986) *Arch. Biochem. Biophys. 246*, 681.
30. delCardayré, S. B., Ribó, M., Yokel, E. M., Quirk, D. J., Rutter, W. J., and Raines, R. T. (1995) *Protein Eng. 8*, 261.
31. Juncosa-Ginestà, M., Pons, J., Planas, A., and Querol, E. (1994) *Biotechniques 16*, 820.
32. Kim, J. S., Soucek, J., Matousek, J., and Raines, R. T. (1995) *J. Biol. Chem. 270*, 10525.
33. Sela, M., and Anfinsen, C. B. (1957) *Biochim. Biophys. Acta 24*, 229.
34. Gill, S. C., and von Hippel, P. H. (1989) *Anal. Biochem. 182*, 319.
35. Lange, R., Frank, J., Saldana, J. L., and Balny, C. (1996) *Eur. Biophys. J. 24*, 277.
36. Silva, J. L., Miles, E. W., and Weber, G. (1986) *Biochemistry* 25, 5780.
37. Deléage, G., and Geourjon, C. (1993) *Comput. Appl. Biosci. 9*, 197.
38. Boix, E., Nogués, M. V., Schein, C. H., Benner, S. A., and Cuchillo, C. M. (1994) *Biol. Chem.* 269, 2529.
39. Leatherbarrow, R. J. (Ed.) (1987) *ENZFITTER: A Non-Linear Regression Data Analysis Program for the IBM-PC*, Elsevier Biosoft, Cambridge.
40. Roussel, A., and Cambilleau, C. (1989) *TURBO−FRODO*, pp 77−79, Silicon Graphics, Mountain View, CA.
41. Wlodawer, A., Svensson, L. A., Sjolin, L., and Gilliland, G. L. (1988) *Biochemistry 27*, 2705.
42. van Gunsteren, W. F., and Berendsen, H. J. C. (1991) *Groningen Molecular Simulations (GROMOS)*, Biomos, Groningen The Netherlands.
43. Xia, T. H. (1992) Ph.D. Dissertation, ETH, Zurich.
44. Kabsch, W., and Sander, C. (1983) *Biopolymers 22*, 2577.
45. Lange, R., Bec, N., Mozhaev, V. V., and Frank, J. (1996) *Eur. Biophys. J. 24*, 284.
46. Elwell, M. L., and Schellman, J. A. (1977) *Biochim. Biophys. Acta 494*, 267.
47. Makhatadze, G. I., and Privalov, P. L. (1995) *Adv. Protein Chem. 47*, 307.
48. Allen, D. L., and Pielak, G. J. (1998) *Protein Sci. 7*, 1262.
49. Serrano, L., Kellis, J. T., Jr., Cann, P., Matouschek, A., and Fersht, A. R. (1992) *J. Mol. Biol. 224*, 783.
50. Shortle, D., Meeker, A. K., and Freire, E. (1988) *Biochemistry 27*, 4761.
51. Juminaga, D., Wedemeyer, W. J., Garduno-Juarez, R., McDonald, M. A., and Scheraga, H. A. (1997) *Biochemistry 36*, 10131.
52. Yamaguchi, T., Yamada, H., and Akasaka, K. (1995) *J. Mol. Biol. 250*, 689.
53. Prehoda, K. E., Mooberry, E. S., and Markley, J. L. (1998) *Biochemistry 37*, 5785.
54. Harpaz, Y., Gerstein, M., and Chothia, C. (1994) *Structure 2*, 641.
55. Pace, C. N., Shirley, B. A., McNutt, M., and Gajiwala, K. (1996) *J. Mol. Biol. 226*, 29.
56. Fauchère, J. L., and Pliska, V. (1983) *Eur. J. Med. Chem. 18*, 369.
57. Sharp, K. A., Nicholls, A., Friedman, R., and Honig, B. (1991) *Biochemistry 30*, 9686.
58. Jackson, S. E., Moracci, M., elMasry, N., Johnson, C. M., and Fersht, A. R. (1993) *Biochemistry 32*, 11259.
59. Nemethy, G., Leach, S. J., and Scheraga, H. A. (1966) *J. Phys. Chem. 70*, 998.
60. Tanford, C. (1980) *The hydrophobic effect*, Wiley & Sons, New York.

BI991460B